Springer

Journal of Mechanical Science and Technology 23 (2009) 3257~3270

Journal of Mechanical Science and Technology

www.springerlink.com/content/1738-494x
DOI 10.1007/s12206-009-1015-y

Dynamic interaction analysis of a LIM train and elevated bridge system †

H. Xia[1,2,*], W. W. Guo[1], C. Y. Xia[1], Y.-L. Pi[2] and M. A. Bradford[2]

[1]*School of Civil Engineering, Beijing Jiaotong University, Beijing 100044, China*
[2]*Center for Infrastructure Engineering & Safety, School of Civil & Environmental Engineering, The University of New South Wales, UNSW Sydney, NSW 2052, Australia*

(Manuscript Received February 6, 2009; Revised June 20, 2009; Accepted September 28, 2009)

Abstract

A three-dimensional dynamic interaction model is developed for a LIM (linear induction motor) train and elevated bridge system, which is composed of a LIM-driven vehicle submodel and a finite element bridge submodel. Each LIM vehicle is modeled by a 27 degrees-of-freedom dynamic system. The expressions for the electromagnetic force between the linear motor and the reaction plate are derived, and the force model is established. By applying a modal superposition technique to the bridge submodel and using the measured track irregularities as the self-excitations of the train-bridge system, the equations of motion are established for analyzing the dynamic responses of the LIM vehicle and the elevated bridge. The proposed framework is applied to a 3-span elevated bridge with 29.9 m simply-supported girders. The full histories of the LIM train traversing the bridge are simulated, from which the dynamic responses of the LIM vehicle and elevated bridge system are obtained. The proposed method may help to find a way to assess the dynamic properties of elevated bridges and the running safety of a LIM train with reasonable computational effort.

Keywords: Linear induction motor; Train; Elevated bridge; Interaction; Dynamic response; Numerical simulation

1. Introduction

Reliable public transport infrastructure is vital to the development of communities. The linear induction motor (LIM or linear motor for short) system, as a new type of urban transit medium [1], offers an array of advanced new features and capabilities. Since the opening of the first LIM line in Canada in 1985, there have been 13 lines completed in 6 countries, with the total length of 320 km. LIM lines are currently under construction in a number of countries. For example, in China, the Beijing Airport Line with a total length of 28.1 km over elevated bridges of 15.75 km length (Fig. 1), and the Guangzhou Metro Line 4 with a total length of 69.67 km over elevated bridges of 48.26 km length have used the LIM system (Fig. 2).

The LIM is driven by a non-adhesion wheel/rail system that does not rely on the friction between the wheels and rails to haul the train [1, 2]. It has advantages in route planning, as LIM trains can easily negotiate steep slopes and sharp curves, thereby reducing the construction costs by requiring smaller route clearances and tunnel cross sections.

The dynamic properties of the LIM system have been studied since 1970's. Several trial LIM lines

Fig. 1. The LIM elevated bridge of Beijing airport line.

† This paper was recommended for publication in revised form by Associate Editor Hong Hee Yoo

*Corresponding author. Tel.: +86 10 82161656, Fax.: +86 10 51683764
E-mail address: hxia88@163.com

Fig. 2. The LIM elevated bridge of metro line 4.

have been established in Japan, Canada, the United States and other countries for theoretical and experimental investigations. Parker [3], Rumsey [4], Teraoka [1] and Matsumaru [2] investigated the development of the LIM system for urban rail transit. Fortin [5] developed a computer simulation method to study the wheel/rail contact relations and the dynamic properties of a LIM bogie on a curved track. Fatemi [6] carried out a dynamic analysis on a LIM track structure with steel sleepers and reaction plate, and investigated variations of the magnetic gap and distribution of motor loads acting on the track, while Hobbs [7] performed a preliminary analysis on the dynamic response and running stability of LIM vehicles In China, the research of LIM systems started in this century, with the planning and the construction of the Guangzhou Metro Line 4 and the Beijing Airport Line. Pang [8] performed a three-dimensional analysis of the linear motor application on a rail-bound vehicle, while Wang [9] established an integral system model for a LIM track on elevated bridges, and analyzed the force and deformation characteristics of the system. Liao and Gao [10] developed a coupled model of a LIM vehicle and slab track system to study the dynamic characteristics of the system under determinate track irregularities. Feng and Wei [11] formulated a spatial dynamic interaction model of a LIM system, and analyzed the dynamic responses of a LIM vehicle and track. Chen and Guo [12] performed a preliminary analysis of the dynamic interaction between the LIM train and elevated bridges, and studied the influence of the train speed, bridge span and pier height on the dynamic response of the bridges.

The dynamic response of railway bridges subjected to moving trainloads is one of the most important engineering problems in bridge design and maintenance. Fundamental theories for bridge structures under moving trains have been reported by a number of researchers, including Frýba [13], Yang and Yau [14], Ju and Lin [15], Fafard *et al.* [16], and Xia [17] among others. Problems concerning multi-span bridges under moving trains have been considered by Cheung *et al.* [18], Matsuura [19], Klasztorny [20], Xia *et al.* [21], and De Roeck and Maeck [22]. On the basis of these studies, the vertical and lateral dynamic responses of bridge structures, and the safety and stability of train vehicles during transit, have been studied and many useful results have been obtained and reported.

As a new type of urban transportation medium, the LIM elevated transit system has distinct dynamic characteristics. The passage of the LIM trains through an elevated railway bridge will induce vibration of the bridge structure, and the vibration of the structure may in turn affect the stability and safety of the moving trains. Therefore, an understanding of the dynamic interaction between LIM trains and elevated bridges is essential for a successful design of the LIM train and elevated bridge system.

In this paper, a three-dimensional dynamic interaction model is developed for a LIM train and elevated bridge system, based on the authors' previous work [17, 21]. Each 2-bogie 4-axle LIM vehicle is modeled as a 27-DOF dynamic system. The expressions for the vertical electromagnetic forces generated between the linear motor and the reaction plate are derived, and a force model for analyzing the vibrations of the LIM vehicle and bridge is formulated. By applying a modal superposition technique to the bridge submodel and using the measured track irregularities as the self-excitations for the train-bridge system, equations of motion are established and a computer code for analyzing the dynamic responses of the elevated bridge and the LIM vehicle is developed. The proposed framework is then applied to a real 3-span elevated bridge with 29.9 m simply-supported girders. The full histories of the LIM train traversing the bridge are simulated by computer, from which the dynamic responses of the LIM vehicle and the elevated bridge are obtained and discussed.

2. Dynamic analysis model of LIM vehicle-bridge system

2.1 LIM vehicle model

2.1.1 Electromagnetic forces in LIM system

When a LIM train moves along a bridge, the train vehicles, bridge girders, piers and their foundations form a complex dynamic interaction system, as shown in Fig. 3. The dynamic analysis model of such

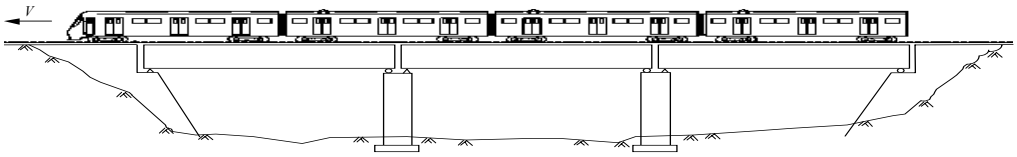

Fig. 3. Dynamic analysis model of train-bridge system.

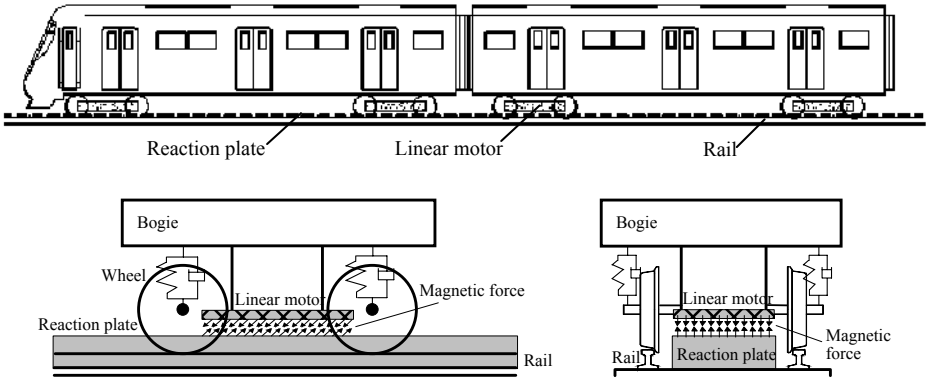

Fig. 4. Working principle of LIM vehicle.

a system is composed of the train submodel, the bridge submodel, the magnetic force model and an assumed wheel-track relationship.

In a linear-motor-driven vehicle, the weight of the vehicle is supported by its wheels, while the propulsion and control are provided by electromagnetic forces. Unlike a conventional rotary motor, the linear motor produces traction and brake forces through linear motion rather than rotary motion. Theoretically, a linear induction motor can be thought of as a rotary motor with an infinite radius. As shown in Fig. 4, a magnetic field (shifting magnetic field) is generated by an alternating current passing to the primary coil (stator in rotary motor) that is mounted on each bogie frame of the cars. At the same time, a magnetic field is also generated in the secondary conductor (reaction plate, rotor in rotary motor), which is fixed to the sleepers along the rail.

In a LIM vehicle, there are two bogies, and each bogie is equipped with a linear motor. The distinct feature of a LIM vehicle is that it is not driven by the adhesion forces between the rail and wheel, with electromagnetic forces between the motor and reaction plate, namely, between the primary coil and secondary conductor. These forces are influenced by the magnetic gap between the linear motor on the vehicle bogie and the reaction plate on the track. Owing to track irregularities, the gap will inevitably vary through the entire traversal of a LIM train. The varying gap may induce a change of magnetic forces acting on the bogie frame and lead it to vibrate. When a LIM train moves along a viaduct bridge, the magnetic gap may vary with the vibration of the vehicle and with the deflections of the bridge, which also leads to varying magnetic forces. The varying magnetic forces may in turn influence the vibration of the bridge and the vehicle, which further changes the magnitude of the magnetic gap. The relationships between the dynamic responses of bridge and vehicles, track irregularities, magnetic gaps and forces are quite complicated. When a LIM train moves on the bridge, the train and the bridge interact and affect each other, and this makes the determination of the magnetic forces and the analysis of the dynamic responses of train-bridge system complex.

The electromagnetic force between the LIM motor and the reaction plate has two components: the longitudinal component that pulls the vehicle to move forward, and the vertical attraction component. In vehicle-bridge system dynamics, the longitudinal vibration is generally neglected; thus only the vertical magnetic forces need to be considered in this analysis. The electromagnetic force is a function of the magnetic gap, the vertical distance between the motor and the reaction plate.

According to the data provided by the Japanese

Subway Society, the relationship between the vertical electromagnetic force and the magnetic gap can be described as [23]

$$f[Z(\xi,\eta)] = 0.3408Z^2(\xi,\eta) - 9.5308Z(\xi,\eta) + 150.02 \quad (1)$$

where $f[Z(\xi,\eta)]$ is the vertical electromagnetic force density (kN/m^2), $Z(\xi, \eta)$ is the magnetic gap (mm), and the coordinate system ξ, η is shown in Fig. 5.

The relationship between the linear motor and the reaction plate at any spatial position is illustrated in Fig. 5. Since the reaction plate is directly mounted on the girder, the vertical displacement of the plate at any position on the girder can be determined by the vertical deflection $Z_b(x)$ and rotational angle $\theta_b(x)$ of the girder, while the vertical displacement of a vehicle bogie at any position can be described using its floating movement Z_{tij}, rolling movement θ_{tij} and pitching movement φ_{tij}. Thus the vertical distance $Z(x,y)$ between the linear motor and the reaction plate at the position of the bogie can be expressed as

$$Z(\xi,\eta) = f[\theta_{tij}, Z_{tij}, \varphi_{tij}, Z_b(x), \theta_b(x)] = [Z_{tij} - Z_b(x)] + \xi\tan\varphi_{tij} + \eta\tan[\theta_{tij} - \theta_b(x)] \quad (2)$$

Thus the vertical, rolling and pitching electromagnetic forces acting at the center of the jth bogie can be obtained from the following equations:

$$\begin{cases} F_M^V = \iint_A f[Z(\xi,\eta)]d\xi d\eta \\ F_M^\theta = \iint_A \eta \cdot f[Z(\xi,\eta)]d\xi d\eta \\ F_M^\varphi = \iint_A \xi \cdot f[Z(\xi,\eta)]d\xi d\eta \end{cases} \quad (3)$$

where A is the horizontal projection area of the linear motor on the reaction plate.

2.1.2 LIM vehicle model

A LIM train is composed of several LIM vehicles. Each vehicle is a multi degree-of-freedom vibration system composed of car body, bogies and wheelsets connected with suspension springs and dashpots as shown in Fig. 6.

The following assumptions are used in the modeling of LIM train vehicles:

(1) The train runs on the bridge at a constant speed so that the degrees-of-freedom of the train vehicles in the longitudinal direction are not included.

(2) The car body, bogies and wheelsets in each vehicle are regarded as rigid components, neglecting their elastic deformation during vibration.

(3) The connections between a car body and its bogies are represented by two linear springs and two viscous dashpots in either the horizontal direction or the vertical direction, respectively, and also the connections between a bogie and its wheelsets.

(4) The ith car body is considered to have five degrees-of-freedom: the lateral Y_{ci}, rolling θ_{ci}, yawing ψ_{ci}, vertical Z_{ci}, and pitching ϕ_{ci} movements. The jth bogie in the ith vehicle has also five degrees-of-freedom: the lateral Y_{tij}, rolling θ_{tij}, yawing ψ_{ti}, vertical Z_{tij}, and pitching φ_{tij} movements. For the lth wheelset in the jth bogie of the ith vehicle (ijlth wheelset for short), only three degrees of freedom: the lateral Y_{wijl}, rolling θ_{wijl} and vertical Z_{wijl} movements are considered.

(5) The linear motor used in the LIM system has a thin rectangular body. The vertical electromagnetic attraction force F_m is developed and expressed by Eqs. (1)~(3).

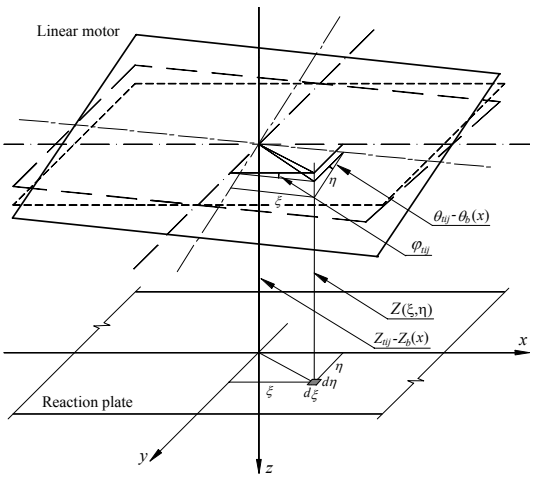

Fig. 5. Relationship between the motor and the reaction plate in spatial positions.

These assumptions greatly simplify the analysis, but still ensure the accuracy of the analysis.

Based on these assumptions, the idealized model for a LIM car with 2 bogies and 4 wheelsets can be described by 27 DOFs, as shown in Fig. 6 and so the equations of motion for the ith vehicle and its two

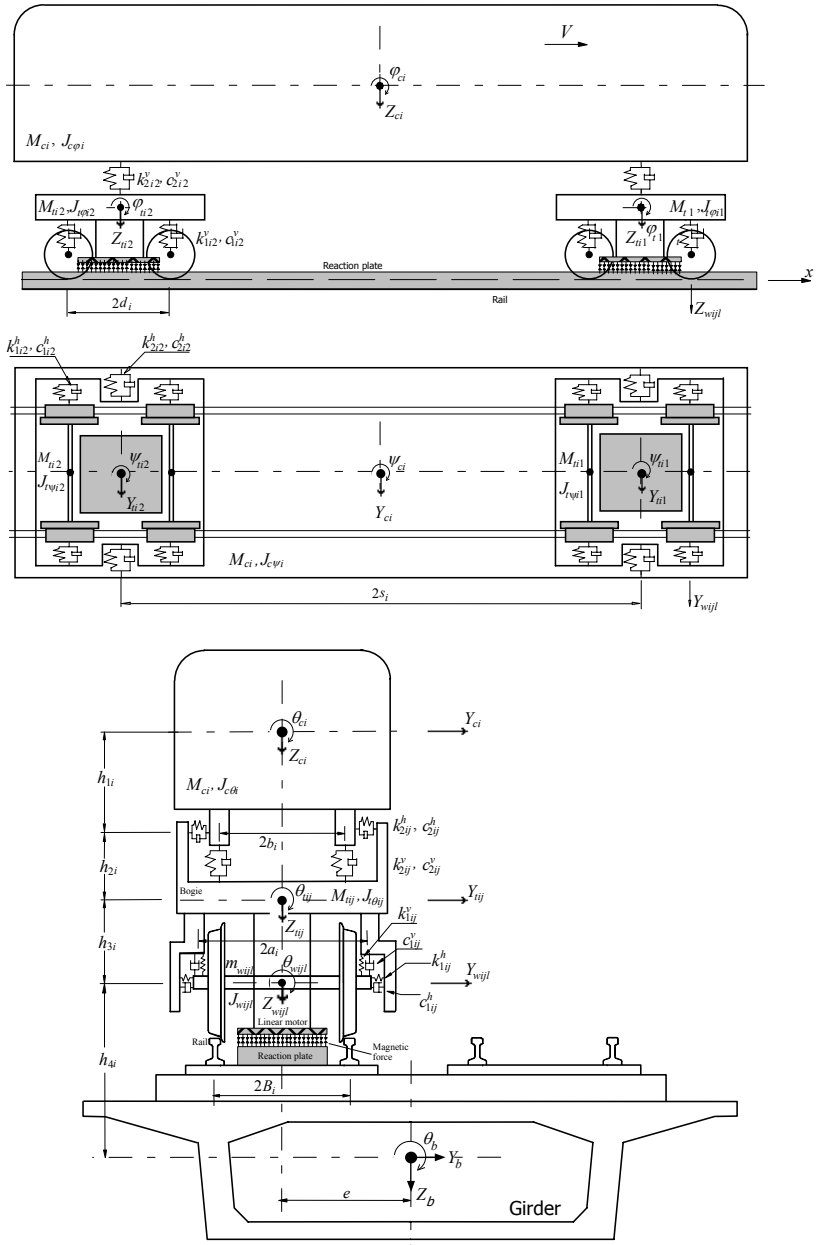

Fig. 6. Dynamic model of linear metro car.

bogies can be expressed as

$$\begin{bmatrix} \mathbf{M}_{\mathrm{cc}\,i} & 0 & 0 \\ 0 & \mathbf{M}_{\mathrm{t_1t_1}\,i} & 0 \\ 0 & 0 & \mathbf{M}_{\mathrm{t_2t_2}\,i} \end{bmatrix} \begin{Bmatrix} \ddot{\mathbf{v}}_{\mathrm{c}\,i} \\ \ddot{\mathbf{v}}_{\mathrm{t_1}\,i} \\ \ddot{\mathbf{v}}_{\mathrm{t_2}\,i} \end{Bmatrix} + \begin{bmatrix} \mathbf{C}_{\mathrm{cc}\,i} & \mathbf{C}_{\mathrm{t_1c}\,i} & \mathbf{C}_{\mathrm{t_2c}\,i} \\ \mathbf{C}_{\mathrm{ct_1}\,i} & \mathbf{C}_{\mathrm{t_1t_1}\,i} & 0 \\ \mathbf{C}_{\mathrm{ct_2}\,i} & 0 & \mathbf{C}_{\mathrm{t_2t_2}\,i} \end{bmatrix} \begin{Bmatrix} \dot{\mathbf{v}}_{\mathrm{c}\,i} \\ \dot{\mathbf{v}}_{\mathrm{t_1}\,i} \\ \dot{\mathbf{v}}_{\mathrm{t_2}\,i} \end{Bmatrix}$$
$$+ \begin{bmatrix} \mathbf{K}_{\mathrm{cc}\,i} & \mathbf{K}_{\mathrm{t_1c}\,i} & \mathbf{K}_{\mathrm{t_2c}\,i} \\ \mathbf{K}_{\mathrm{ct_1}\,i} & \mathbf{K}_{\mathrm{t_1t_1}\,i} & 0 \\ \mathbf{K}_{\mathrm{ct_2}\,i} & 0 & \mathbf{K}_{\mathrm{t_2t_2}\,i} \end{bmatrix} \begin{Bmatrix} \mathbf{v}_{\mathrm{c}\,i} \\ \mathbf{v}_{\mathrm{t_1}\,i} \\ \mathbf{v}_{\mathrm{t_2}\,i} \end{Bmatrix} = \begin{Bmatrix} 0 \\ \mathbf{F}_{\mathrm{t_1}\,\mathrm{v}\,i} \\ \mathbf{F}_{\mathrm{t_2}\,\mathrm{v}\,i} \end{Bmatrix} \tag{4}$$

where i = 1, 2,…, N_{v}, and N_{v} is the number of vehicles on the bridge; the superscripts c, t_1 and t_2 represent the car body, and the front and rear bogies of the vehicle, respectively; $\boldsymbol{M}$, $\boldsymbol{K}$ and $\boldsymbol{C}$ are the mass, stiffness and damping matrices, respectively; $\mathbf{v}_i$, $\dot{\mathbf{v}}_i$ and $\ddot{\mathbf{v}}_i$ are the displacement, velocity and acceleration vectors of the ith vehicle, respectively.

The force vector from the wheelsets acting on the jth bogie of the ith vehicle can be written as

$$\mathbf{F}_{vi}^{tj}=\sum_{l=1}^{N_{wi}}\begin{Bmatrix}k_{1ij}^{h}Y_s(x_{ijl})+c_{1ij}^{h}\dot{Y}_s(x_{ijl})\\ a_i^2[k_{1ij}^{v}\theta_s(x_{ijl})+c_{1ij}^{v}\dot{\theta}_s(x_{ijl})]\\ \quad -h_{3i}[k_{1ij}^{h}Y_s(x_{ijl})+c_{1ij}^{h}\dot{Y}_s(x_{ijl})]\\ \eta_l d_i[k_{1ij}^{h}Y_s(x_{ijl})+c_{1ij}^{h}\dot{Y}_s(x_{ijl})]\\ k_{1ij}^{v}Z_s(x_{ijl})+c_{1ij}^{v}Z_s(x_{ijl})\\ \eta_l d_i[k_{1ij}^{v}Z_s(x_{ijl})+c_{1ij}^{v}\dot{Z}_s(x_{ijl})]\end{Bmatrix}+\begin{Bmatrix}0\\ F_{Mj}^{\theta}\\ 0\\ F_{Mj}^{V}\\ F_{Mj}^{\varphi}\end{Bmatrix} \tag{5}$$

where N_{wi} is the number of wheelsets in the jth bogie of the ith vehicle; $Y_s(x_{ijl})$, $Z_s(x_{ijl})$, and $\theta_s(x_{ijl})$ are the lateral, vertical, and rotational track irregularities at the position of the ijlth wheelset , respectively, η_l is the sign function, η_l =1 when the lth wheelset is in the front bogie and η_l = -1 the lth wheelset is in the rear bogie; a_i , b_i , d_i and s_i are the longitudinal and lateral distances between the axes of the ith vehicle, as shown in Fig. 6, F_{Mj}^{V}, F_{Mj}^{θ} and F_{Mj}^{φ} are the vertical, rolling and pitching electromagnetic forces of the jth bogie defined in Eq. (3).

2.2 Wheel/bridge interface model

This study assumes that there is no relative displacement between the track and bridge deck. The elastic effects of the track system are also neglected.

The bridge deck is modeled as a three-dimensional system using the finite element method and the equation of motion for the bridge deck can be expressed as

$$\mathbf{M}\ddot{\mathbf{X}}+\mathbf{C}\dot{\mathbf{X}}+\mathbf{K}\mathbf{X}=\mathbf{F} \tag{6}$$

where $\boldsymbol{M}$, $\boldsymbol{C}$, and $\boldsymbol{K}$ are the mass, damping and stiffness matrices of the bridge deck; $\ddot{\mathbf{X}}$, $\dot{\mathbf{X}}$ and $\boldsymbol{X}$ are the acceleration, velocity and displacement vectors of the bridge deck, respectively; and $\boldsymbol{F}$ is the force vector, consisting of two parts:

$$\mathbf{F}=\mathbf{F}_W+\mathbf{F}_M \tag{7}$$

where $\boldsymbol{F}_W$ is the vector of forces from the wheels of a train on the bridge deck through the track and $\boldsymbol{F}_M$ is the vector of electromagnetic forces. The displacements of an arbitrary point of the cross-section of bridge deck are usually described by the lateral displacement $\boldsymbol{Y}_b$, vertical displacement $\boldsymbol{Z}_b$, and torsional displacement $\boldsymbol{\theta}_b$ at the centroid of the cross section. The lateral, vertical and torsional forces of the ijlth wheelset corresponding to the deck displacements can be derived from the equilibrium conditions of the wheelset and the relative position of the track to the bridge deck cross section as

$$\begin{cases}F_{hijl}=-m_{wijl}\ddot{Y}_{wijl}+c_{1ij}^{h}(\dot{Y}_{t_ji}-h_{3i}\dot{\theta}_{t_ji}+2\eta_l d_i\dot{\psi}_{t_ji}-\dot{Y}_{wijl})\\ \qquad +k_{1ij}^{h}(Y_{t_ji}-h_{3i}\theta_{t_ji}+2\eta_l d_i\psi_{t_ji}-Y_{wijl})\\ F_{vijl}=-m_{wijl}\ddot{Z}_{wijl}+c_{1ij}^{v}(\dot{Z}_{t_ji}+2\eta_l d_i\dot{\varphi}_{t_ji}-\dot{Z}_{wijl})\\ \qquad +k_{1ij}^{v}(Z_{t_ji}+2\eta_l d_i\varphi_{t_ji}-Z_{wijl})\\ \qquad +g[m_{wijl}+(0.5M_{ci}+M_{t_ji})/N_{wij}]\\ F_{\theta ijl}=-J_{wijl}\ddot{\theta}_{wijl}+2a_i^2c_{1ij}^{v}(\dot{\theta}_{t_ji}-\dot{\theta}_{wijl})\\ \qquad +2a_i^2k_{1ij}^{v}(\theta_{t_ji}-\theta_{wijl})+h_{4i}F_{hijl}+e_iF_{vijl}\end{cases} \tag{8}$$

where m_{wijl} and J_{wijl} are the mass and the mass moment of the ijlth wheel, respectively; g is the acceleration due to gravity; and h_{4i} and e are the distances shown in Fig. 6.

That the vector of electromagnetic forces $\boldsymbol{F}_M$ induced by the jth bogie can be expressed as

$$\begin{aligned}\mathbf{F}_M&=\begin{cases}0\\ -F_{Mj}^{V}\\ F_{Mj}^{\theta}+e\cdot F_{Mj}^{V}\end{cases}\\ &=\begin{cases}0\\ -\iint_A f[Z_j(\xi,\eta)]\mathrm{d}\xi\mathrm{d}\eta\\ \iint_A \eta\cdot f[Z_j(\xi,\eta)]\mathrm{d}\xi\mathrm{d}\eta+e\cdot\iint_A f[Z_j(\xi,\eta)]\mathrm{d}\xi\mathrm{d}\eta\end{cases}\end{aligned} \tag{9}$$

where F_{Mj}^{V} and F_{Mj}^{θ} are the vertical and rotational electromagnetic forces induced by the jth vehicle bogie, as described in detail in Fig. 5 and Eqs. (2)-(3).

2.3 Dynamic model for LIM train-bridge system

This study is concerned with the dynamic interaction between the bridge and the LIM train without external excitations such as wind or earthquake. The equation of motion for the train given by Eq. (4) and the equation of motion for the bridge given by Eq. (6) form the basic equations of motion for the coupled bridge-train system. However, the direct integration

of these equations in the time domain for the dynamic responses of the both bridge and train is very cumbersome. In addition, the elastic deformations of the bridge are sufficient for analyzing the dynamic interactive responses of the train-bridge system. Therefore, the modal analysis method can be adopted for modelling the bridge subsystem. To include the effects of both the global deformation of the bridge and the local deformation of the structural elements that support the track, a sufficiently large number of modal shapes of the bridge deck are needed. The minimum number of modes can be determined by studies of the convergence of the effects of different mode numbers, or by comparisons with measured data. The modal shape between the deck nodes is determined using Lagrange interpolation from those obtained from the eigenvalue analysis.

Let $\phi_{\mathrm{h}}^{n}(x_{ijl})$, $\phi_{\theta}^{n}(x_{ijl})$ and $\phi_{\mathrm{v}}^{n}(x_{ijl})$ denote the lateral, rotational and vertical components of the nth bridge mode at the position of the ijlth wheel, and q_n denote the nth generalized coordinate. The displacement responses of the bridge deck can then be expressed as

$$\begin{cases} Y_{\mathrm{b}}(x_{ijl}) = \sum_{n=1}^{N_{\mathrm{b}}} q_n \phi_h^n(x_{ijl}) \\ \theta_{\mathrm{b}}(x_{ijl}) = \sum_{n=1}^{N_{\mathrm{b}}} q_n \phi_\theta^n(x_{ijl}) \\ Z_{\mathrm{b}}(x_{ijl}) = \sum_{n=1}^{N_{\mathrm{b}}} q_n \phi_v^n(x_{ijl}) \end{cases} \tag{10}$$

where N_{b} is the number of modes. The modal equation of motion of the bridge deck can be obtained on Eq. (6) as

$$M_n \ddot{q}_n + C_n \dot{q}_n + K_n X_n = F_n \tag{11}$$

where n denotes the nth mode, M_n, C_n and K_n are generalized mass, damping and stiffness matrices respectively, F_n is generalized force vector.

Deviations of the real rail from the ideal perfect rail are due mainly to the track irregularity, which is an important self-excitation in the bridge-train system in addition to the moving gravity load of the train. Measured track irregularities are assumed to be given, and so the relationship between displacements of the ijlth wheelset and movements of the bridge deck can be expressed as

$$\begin{Bmatrix} Y_w(x_{ijl}) \\ \theta_w(x_{ijl}) \\ Z_w(x_{ijl}) \end{Bmatrix} = \begin{Bmatrix} Y_b(x_{ijl}) + h_{4i} \cdot \theta_b(x_{ijl}) + Y_s(x_{ijl}) \\ \theta_b(x_{ijl}) + \theta_s(x_{ijl}) \\ Z_b(x_{ijl}) + e \cdot \theta_b(x_{ijl}) + Z_s(x_{ijl}) \end{Bmatrix} \tag{12}$$

where x_{ijl} is the position of the ijlth wheelset on the bridge, and e the eccentric distance of the track on the girder.

Substituting Eq. (12) to Eq. (8), and then to Eqs. (4) and (5) leads to the coupled equations of motion for the bridge-train system as

$$\begin{bmatrix} \mathbf{M}_{\mathrm{vv}} & 0 \\ 0 & \mathbf{M}_{\mathrm{bb}} \end{bmatrix} \begin{Bmatrix} \ddot{\mathbf{X}}_{\mathrm{v}} \\ \ddot{\mathbf{X}}_{\mathrm{b}} \end{Bmatrix} + \begin{bmatrix} \mathbf{C}_{\mathrm{vv}} & \mathbf{C}_{\mathrm{vb}} \\ \mathbf{C}_{\mathrm{bv}} & \mathbf{C}_{\mathrm{bb}} \end{bmatrix} \begin{Bmatrix} \dot{\mathbf{X}}_{\mathrm{v}} \\ \dot{\mathbf{X}}_{\mathrm{b}} \end{Bmatrix} + \begin{bmatrix} \mathbf{K}_{\mathrm{vv}} & \mathbf{K}_{\mathrm{vb}} \\ \mathbf{K}_{\mathrm{bv}} & \mathbf{K}_{\mathrm{bb}} \end{bmatrix} \begin{Bmatrix} \mathbf{X}_{\mathrm{v}} \\ \mathbf{X}_{\mathrm{b}} \end{Bmatrix} = \begin{Bmatrix} \mathbf{F}_{\mathrm{v}} \\ \mathbf{F}_{\mathrm{b}} \end{Bmatrix} \tag{13}$$

where the subscripts v and b denote vehicles and the bridge, respectively, $\boldsymbol{M}$, $\boldsymbol{C}$ and $\boldsymbol{K}$ are the mass, damping and stiffness matrices, and $\boldsymbol{F}_{\mathrm{v}}$ and $\boldsymbol{F}_{\mathrm{b}}$ are the force vectors acting on the vehicles and the bridge, respectively. Details of the mass, damping, stiffness matrices and displacement vector are the same as those in a train-bridge system developed by authors elsewhere [17, 21].

The force vector $\boldsymbol{F}_{\mathrm{v}}$ acting on the vehicles can be expressed as

$$\mathbf{F}_{\mathrm{v}} = [\mathbf{F}_{\mathrm{v}1} \quad \mathbf{F}_{\mathrm{v}2} \quad \cdots \quad \mathbf{F}_{\mathrm{v}N_v}]^{\mathrm{T}} \tag{14}$$

where $\mathbf{F}_{\mathrm{v}i} = \begin{bmatrix} 0 & \mathbf{F}_{\mathrm{v}i}^{t_1} & \mathbf{F}_{\mathrm{v}i}^{t_2} \end{bmatrix}^{\mathrm{T}}$, ($i$=1, 2, ⋯, N_{v}), is the force vector of the ith vehicle, which is found by Eqs. (4) and (5), and N_{v} is the number of vehicles traversing on the bridge.

The modal force vector of the bridge $\boldsymbol{F}_{\mathrm{b}}$ can be written as

$$\mathbf{F}_{\mathrm{b}} = [F_b^1 \quad F_b^2 \quad \cdots \quad F_b^{Nq}]^{\mathrm{T}} \tag{15}$$

where N_{q} denotes the mode number used in the analysis, and F_{b}^{n} (n=1,2, ⋯, N_{q}) is the generalized force of the nth mode as

$$F_b^n = F_{bW}^n + F_{bM}^n \tag{16}$$

and $F_{\mathrm{b}W}^{n}$ is the generalized force transmitted from all the vehicle wheels to the bridge and given by

$$F_{b\mathrm{W}}^{n}=\sum_{i=1}^{N_v}\sum_{j=1}^{2}\sum_{l=1}^{N_{wi}}[\phi_{\mathrm{h}}^{n}(x_{ijl})\cdot F_{hijl}+\phi_{\mathrm{v}}^{n}(x_{ijl})\cdot F_{vijl}+\phi_{\theta}^{n}(x_{ijl})\cdot F_{\theta ijl}]$$
$$=\sum_{i=1}^{N_v}\sum_{j=1}^{2}\sum_{l=1}^{N_{wi}}\Big\{[\phi_{\mathrm{h}}^{n}(x_{ijl})+h_{4i}\cdot\phi_{\theta}^{n}(x_{ijl})]\cdot k_{1ij}^{h}\cdot Y_s(x_{ijl})+2\phi_{0}^{n}(x_{ijl})\cdot k_{1ij}^{v}\cdot a_i^2\cdot\theta_s(x_{ijl})+[\phi_{\mathrm{v}}^{n}(x_{ijl})+e_i\cdot\phi_{0}^{n}(x_{ijl})]\times\Big[k_{1ij}^{v}\cdot Z_s(x_{ijl})+g\cdot[m_{wijl}+(0.5M_{ci}+M_{tij})/N_{wij}]\Big]\Big\} \tag{17}$$

where F_{hijl}, F_{vijl} and $F_{\theta ijl}$ are, respectively, the lateral, vertical and torsional forces of the ijlth wheelset given in Eq. (8); and $F_{\mathrm{b}W}^{n}$ is the generalized magnetic force from all bogies and is expressed as

$$F_{\mathrm{b}M}^{n}=\sum_{i=1}^{N_v}\sum_{j=1}^{2}\Big\{-\phi_{\mathrm{v}}^{n}(x_{ij})F_{\mathrm{M}j}^{\mathrm{V}}+\phi_{\theta}^{n}(x_{ij})[e\cdot F_{\mathrm{M}j}^{\mathrm{V}}+F_{\mathrm{M}j}^{\theta}]\Big\} \tag{18}$$

Eq. (13) is a second-order linear non-homogeneous differential equations with time-varying coefficients. These equations are solved using the Newmark implicit integral algorithm [24] with β=1/4 in this study.

A computer code for the coupled train-bridge system is developed based on the formulations in this investigation and is used to perform a case study as follows.

3. Case study

3.1 Bridge and train parameters

The case study concerns an elevated subway bridge and a LIM train. As shown in Fig. 7, the bridge consists of three 29.9 m span simply-supported concrete box girders with two 10m high piers, carrying two LIM tracks on the bridge deck. The girder has a trapezium section with a total height of 1.7 m, top width of 9.3 m and a bottom width of 3.99 m. The secondary load used in the calculation is 76.0 kN/m.

The LIM train consists of four LIM vehicles and each vehicle has two identical bogies supported by two identical wheelsets. The design train speed is 70km/h, and the train speeds used in calculation are 50~90km/h. The dimension of the LIM motor is 240cm×36cm, the design magnetic gap is 10 mm, and the design electromagnetic force is 31.96 kN. The average static axle loads are 74.95 kN (tare) and 109.38 kN (crush). The main parameters of the vehicle in study are listed in Table 1.

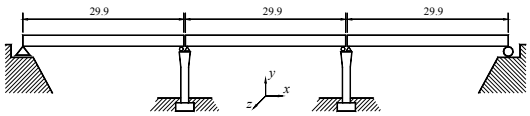

(a) Elevation of the bridge

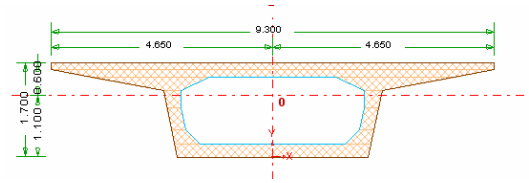

(b) Cross section of girder

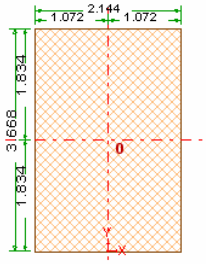

(c) Cross section of pier

Fig. 7. Dimensions of the bridge.

3.2 Track irregularities

As noted, track irregularity plays an important role in the dynamic analysis of the train-track interactive system, which is the main excitation that induces the train-bridge system to vibrate. It is also a control factor to influence the running safety and stability of vehicles, and a main cause of structural damage and faults of the track components.

To obtain the track irregularity, a measurement was carried out by the authors on the irregularity of tracks on the elevated bridge on Beijing Metro Line 5. The statistical standard variation of the track irregularities and the power spectrum were calculated by the following formulas [25]:

$$\sigma_{\eta}^{2}=\frac{1}{X}\int_{0}^{x}\left[\eta(x)-\mu_{\eta}\right]^{2}\mathrm{d}x=\varphi_{\eta}^{2}-\mu_{\eta}^{2} \tag{19}$$

$$S_{\eta}(f)=\lim_{\Delta f\to\infty}\frac{1}{\Delta f}\left[\lim_{X\to\infty}\frac{1}{X}\int_{0}^{X}\eta^{2}(x,f,\Delta f)\mathrm{d}x\right] \tag{20}$$

where $\eta(x)$ is the profile, μ_{η} is the mean, X is the total sampling length, f is the space frequency, and Δf

Table 1. Main parameters of vehicle used in the case study.

Parameter	Value
Full length of a coach L (m)	18.37
Distance between two bogies $2s$ (m)	11.14
Distance between two wheelsets $2d$ (m)	2.0
Mass of car body M_c (t)	33.45
Roll mass moment of car body $J_{c\theta}$ (t-m^2)	35.0
Pitch mass moment of car body $J_{c\varphi}$ (t-m^2)	150.0
Yaw mass moment of car body $J_{c\psi}$ (t-m^2)	145.0
Mass of bogie M_t (t)	2.85
Roll mass moment of bogie $J_{t\theta}$ (t-m^2)	0.7
Pitch mass moment of bogie $J_{t\varphi}$ (t-m^2)	0.6
Yaw mass moment of bogie $J_{t\psi}$ (t-m^2)	0.8
Mass of wheelset m_w (t)	1.15
Roll mass moment of wheelset J_w (t-m^2)	1.12
Primary vertical spring stiffness k_1^v (kN/m)	2000
Primary lateral spring stiffness k_1^h (kN/m)	14000
Secondary vertical spring stiffness k_2^v (kN/m)	300
Secondary lateral spring stiffness k_2^h (kN/m)	250
Primary vertical dashpot c_1^v (kNs/m)	100
Primary lateral dashpot c_1^h (kNs/m)	700
Secondary vertical dashpot c_2^v (kNs/m))	30
Secondary lateral dashpot c_2^h (kNs/m)	25
Distance h_1(m)	0.64
Distance h_2 (m)	0.46
Distance h_3 (m)	0.085
Distance h_4 (m)	1.125
Distance $2a$ (m)	1.15
Distance $2b$ (m)	1.56
Distance $2B$ (m)	1.435
Distance e (m)	2.05

is the frequency interval of track irregularity. Fig. 8 shows the power spectra of the lateral and vertical rail irregularities, by which the track irregularity series are numerically generated using the method given in [17, 25].

3.3 Results

The ANSYS software was used in establishing the finite element model of the bridge, with the girders and piers being discretized by using beam elements, and the secondary loads of the bridge distributed on the girders as a supplementary mass. The natural vibration properties of the bridge were analyzed and there are altogether 40 frequencies and mode shapes

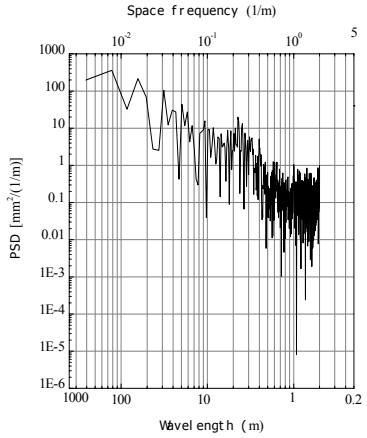

(a) Lateral

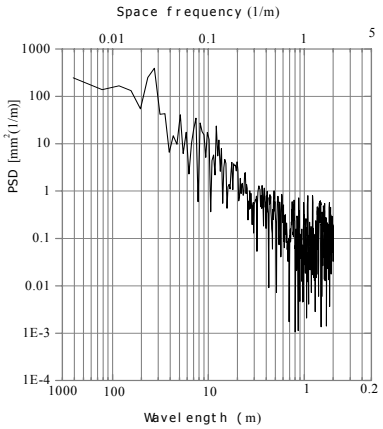

(b) Vertical

Fig. 8. Power spectra of measured track irregularities.

obtained for such a three-span bridge, and were included in the calculation. The first lateral and vertical frequencies of the girders are 3.05 Hz and 3.16 Hz, respectively.

The damping ratio of the bridge structure is assumed to be 2%, and was used in Eq. (6) as the Rayleigh damping. The integration time step is taken as 0.001s.

3.3.1 Variation of electromagnetic forces

As indicated in Eq. (1), the electromagnetic force is governed by the magnetic gap. The calculated time-history of the magnetic gap generated by the linear motor on the first bogie is shown in Fig. 9, when the train has a constant speed of 70 km/h. It can be seen that a train running on the bridge induces a larger variation of the magnetic gap than when it runs on the ground track.

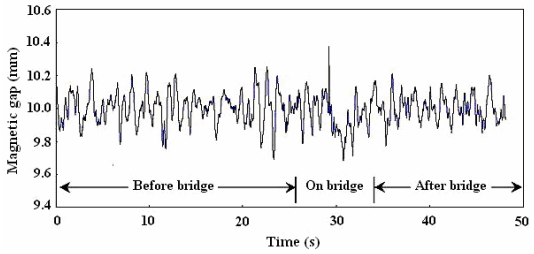

Fig. 9. Time-history of magnetic gap generated by the first motor.

3.3.2 Responses of an elevated bridge

Time histories of the lateral and vertical displacement and acceleration responses of the bridge girder at its mid-span, when the train on the bridge has a speed of 70 km/h, are shown in Figs. 10 and 11, respectively. It can be seen that the vertical dynamic displacement response is similar to the static influence line under running trains, and that the maximum response is 4.11 mm. This shows that the vertical deflection of the bridge under the train is mainly induced by the gravity loading of the moving train vehicles. Compared with the vertical responses, the lateral displacements of the bridge are quite small with a maximum of 0.042 mm, and include more high frequency components. The lateral acceleration of the bridge is smaller than that of the vertical one, but with higher frequencies.

Variations of the distributions of the maximum bridge mid-span responses with the train speed are shown in Figs. 12 and 13, respectively. The results show that within the train speed range of 50~90 km/h, the maximum lateral displacement and accelerations of the bridge increase with the train speed, while the vertical responses reach their crest values at the train speed of 70km/h. This is because the speed of 70km/h is very close to the resonant train speed for a simply-supported girder estimated by Eq. (20) [17, 25].

$$V_{\mathrm{br}} = \frac{3.6 \cdot f_{\mathrm{b}}^{n} \cdot d_{\mathrm{v}}}{i} \qquad (n = 1,2,3\cdots; i = 1,2,3\cdots) \quad (20)$$

where: V_{br} is the resonance train speed of the bridge (km/h); f_{b}^{n} is the nth vertical natural frequency of the bridge (Hz); d_{v} is the load interval (m). Since the first natural frequency of the girder is f_{b}^{1}=3.16 Hz, and the full length of the vehicle d_{v}=18.37 m, when i=3, the resonance train speed can be obtained as V_{br} =69.66 km/h.

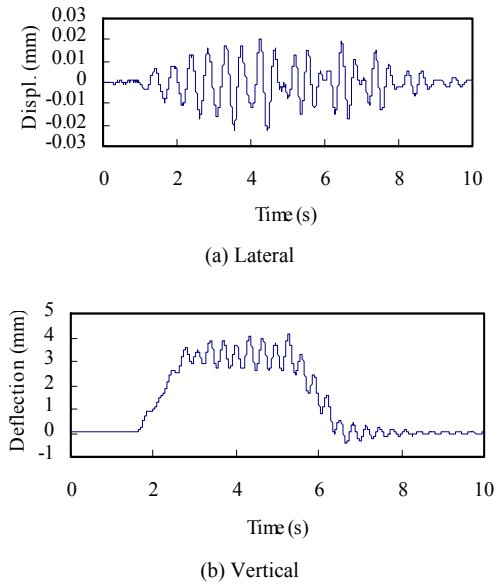

Fig. 10. Mid-span displacement histories of girder.

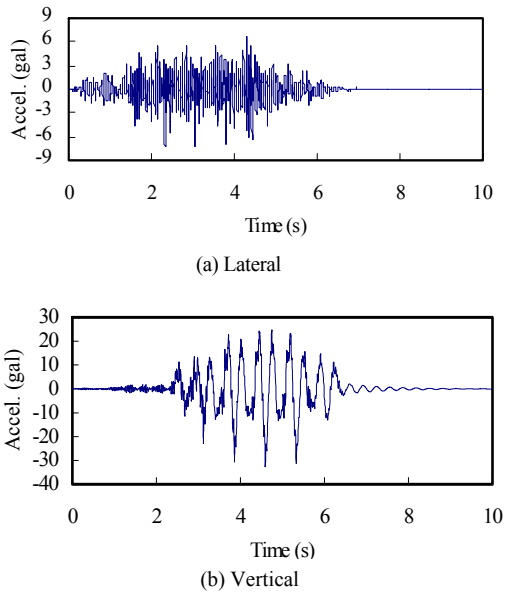

Fig. 11. Mid-span acceleration histories of girder.

It can also be seen from Figs. 12 and 13 that both the vertical deflections and accelerations induced by a crush loaded train (AW2) are greater than those induced by tare loaded trains (AW0), while the differences for the lateral responses are quite small.

Listed in Table 2 are the maximum responses of the bridge under the train speed range of 50~90 km/h, and the corresponding allowances given by the Chinese Railway Code.

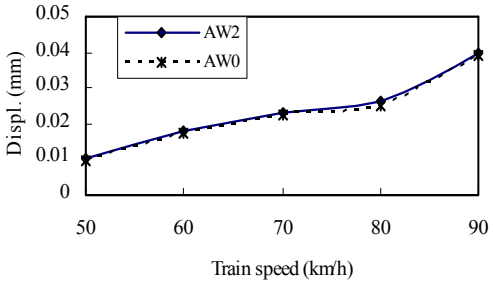

(a) Lateral

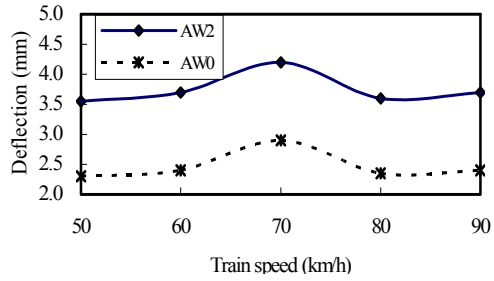

(b) Vertical

Fig. 12. Maximum bridge displacements vs train speed.

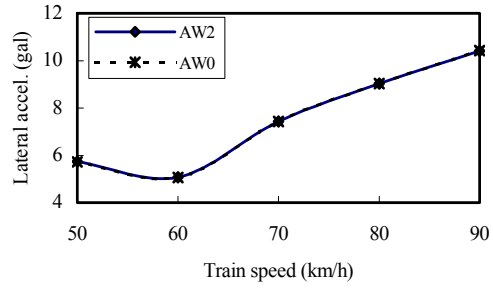

(a) Lateral

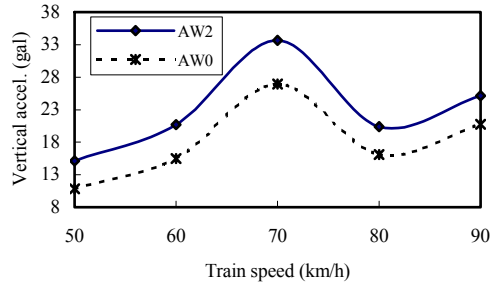

(b) Vertical

Fig. 13. Maximum bridge accelerations vs train speed.

It can be seen that the maximum deflection of the girder is 4.11 mm, occurring at the train speed of 70 km/h, and the corresponding deflection-to-span ratio is about 1/7300.

Table 2. Maximum responses of bridge girder.

Bridge response		Allowance	Vehicle load	
			AW2 (Crush load)	AW0 (Tare load)
Displacement (mm)	Vertical	15.0	4.11	2.69
	Lateral	0.15	0.04	0.039
Acceleration (cm/s^2)	Vertical	500	33.69	26.98
	Lateral	--	10.42	10.42

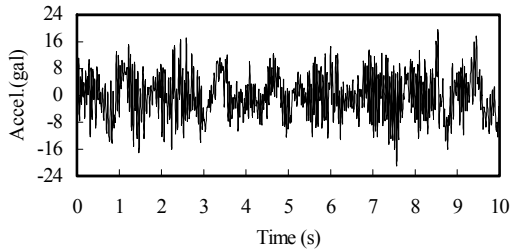

(a) Lateral

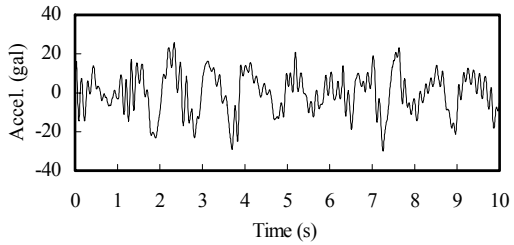

(b) Vertical

Fig. 14. Acceleration time histories of car-body.

When the LIM train runs on the bridge, all the dynamic responses of the bridge are much smaller than the allowable values given in the Chinese Code.

3.3.3 Responses of LIM vehicle

Time histories of the accelerations of the vehicle car-body when the train runs on the bridge at a speed of 70 km/h are shown in Fig. 14.

It can be found from Fig. 14 that the vertical acceleration of the vehicle is only slightly larger than the lateral response, but the pattern of the vertical acceleration time histories are different from that of the lateral response to some extent. The maximum acceleration responses in both directions are well below the allowable accelerations related to human comfort. It is also found that the lateral and vertical responses of the car body as the vehicle runs on the bridge are similar to those when the vehicle runs on the ground. This indicates that the motion of the bridge does not

strongly affect the human comfort within the vehicles. As a result, the track irregularities dominate the responses of the car body and these responses seem to be random.

There are two important parameters that should be considered for the evaluation of the safety of the train vehicles: the derailment factor Q/P and the offloading factor ΔP/P.

Fig. 15 shows the time histories of these two responses of a vehicle as the train runs on the bridge, while Figs. 16-17 show variations of the distributions of the maximum vehicle responses with the train speed, respectively.

The results show that the dynamic responses of the train vehicles are influenced by the train speed. Within the train speed range of 50~90 km/h, the maximum vertical and lateral car-body accelerations, the derailment factor and the offload factor of the vehicle increase with the train speed. The derailment factors and offload factors of the vehicle under tare loads are noticeably greater than those under crush loads, but the differences between the vehicle car-body accelerations are small. This indicates that for the running safety and stability, the tare train is more unfavorable than the crush one.

Table 3 lists the maximum responses of the train vehicles under the train speed range of 50~90 km/h, and the corresponding allowances given by the Chinese Railway Code.

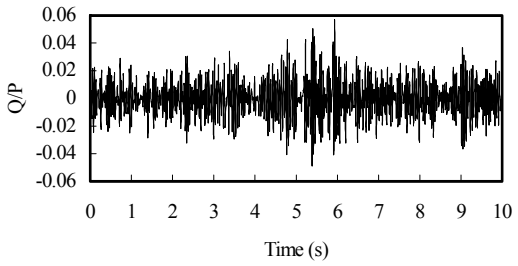

(a) Derailment factor

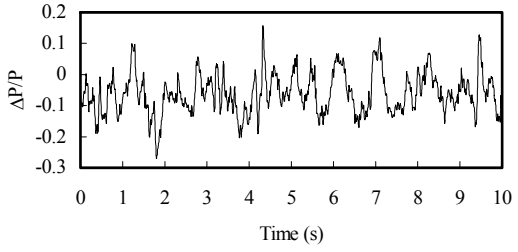

(b) Offload factor

Fig. 15. Dynamic response histories of vehicle wheel.

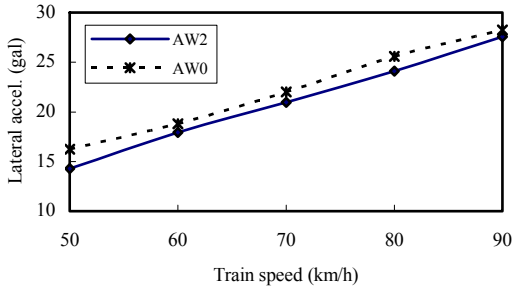

(a) Lateral

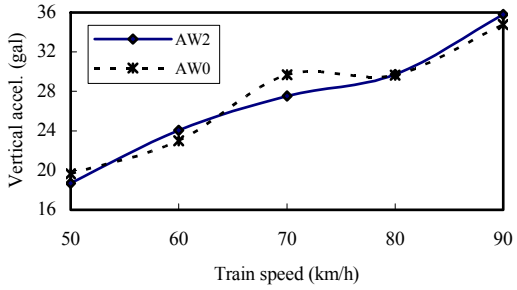

(b) Vertical

Fig. 16. Maximum car-body accelerations vs train speed.

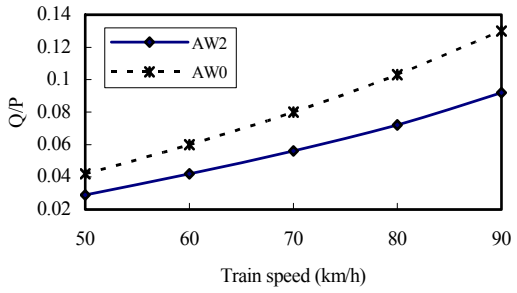

(a) Derailment factor

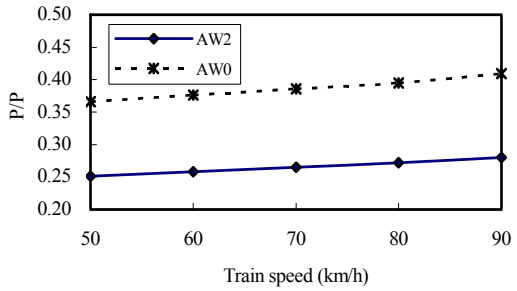

(b) Offload factor

Fig. 17. Maximum vehicle safety indices vs train speed.

Table 3. Maximum responses of vehicles.

Vehicle response		Allowance	Vehicle load	
			AW2 (Crush load)	AW0 (Tare load)
Car-body acceleration (cm/s^2)	Vertical	200	35.78	34.78
	Lateral	150	27.56	28.25
Derailment factor Q/P		0.80	0.092	0.130
Offload factor ΔP/P		0.60	0.280	0.409

It can be seen that when the train runs on the bridge, the dynamic responses of LIM vehicles can satisfy the running safety and stability requirements. Due to the existence of the attractive electromagnetic force, the derailment factors of LIM vehicle are much smaller than those of the conventional train vehicles, showing very good running properties.

4. Conclusions

A framework for performing dynamic analysis of a coupled train and bridge in a LIM system has been established and applied to an elevated bridge as a case study. The full time histories of the dynamic responses for the bridge and LIM train traversing the bridge have been computed. The dynamic responses of the bridge such in terms of the mid-span displacements and accelerations, and those of the train vehicles such as car-body accelerations, derailment factors and offload factors have been obtained. The results show that the dynamic responses of the elevated bridge and the LIM train vehicles are excellent, which shows that the LIM system possesses attractive prospects for development in this regard.

The proposed method may help to find a way to assess the dynamic behavior of the elevated bridge and the linear metro vehicles in the time domain with reasonable computational effort.

Acknowledgment

This research is supported by a key project awarded by the Natural Science Foundation of China (No. 50838006), a project awarded by the Natural Scientific Foundation of Beijing (No. 8082021), and a Flander (Belgium)-China bilateral project (No. BIL07/07).

References

[1] S. Teraoka, Adoption of linear motor propulsion system for subway, *Proc. of the 15th International Conference on MAGLEV*, (1998) 140-146.

[2] H. Matsumaru, Hitachi Contributes to railway systems for the 21st century. *Hitachi Review*. 48 (3) (1999) 124-125.

[3] J. Parker and G. Dawson, LIM propulsion system development for transit. *IEEE Transactions on Magnetics*. 15 (6) (1979) 311-317.

[4] A. Rumsey, A. Wallace and A. Jeffries, Propulsion and control consideration on intermediate capacity transit system. *IEEE Industry Applications Society Annual Meeting*. (1981) 274-277.

[5] C. Fortin, *Dynamic curbing simulation of forced-steering rail vehicles*. Dissertation, Kingston, Ontario: Queen's University, (1985).

[6] M. Fatemi, *Resilient cross-tie track for a transit guideway*. Dissertation, Kingston, Ontario: Queen's University, (1993).

[7] A. Hobbs and T. Pearce, Lateral dynamics of the linear induction motor test vehicle. *Journal of Dynamic Systems, Measurement and Control*. 90 (1994) 221-232.

[8] S. H. Pang and M. Geng, Three-dimensional analysis of linear motor application on rail bound vehicle. *Electric Locomotives & Mass Transit Vehicles*, 27 (1) (2004) 31-33.

[9] K. L. Wang. *Study on some key track technologies for LIM metro system*. Dissertation, Beijing: Beijing Jaitong University, (2005).

[10] L. Liao and L. Gao, A dynamics coupling model for vehicle-slab track in LIM transit system. *J. Urban Railway Transit*. 19 (2) (2006) 22-26.

[11] Y. W. Feng and Q. C. Wei, A vertical model for vehicle-track coupling dynamics on linear metro system. *Journal of Beijing Jiaotong University*, 30 (1) (2006) 51-54.

[12] J. W. Chen and W. W. Guo, An analysis on dynamic interaction of linear induction motor (LIM) train and elevated bridge system. *J. Urban Rapid Rail Transit*, 19 (1) (2006) 44-48.

[13] L. Frýba, *Vibration of solids and structures under moving loads*, London: Thomas Telford, (1999).

[14] Y. B. Yang and J. D. Yau, Vehicle-bridge interaction element for dynamic analysis. *J Structural Engineering ASCE*. 123 (11) (1997) 1512-1518.

[15] S. H. Ju and H. T. Lin, Resonance characteristics of high-speed trains passing simply supported bridges. *J Sound and Vibration*. 267 (2003) 1127-1141.

[16] M. Fafard, A. Mallikarjun and M. Savard, Dynam-

ics of bridge vehicle interaction. *Proc EURODYN'93*, Trondheim, (1993) 951-960.

[17] H. Xia and N. Zhang, *Dynamic interaction of vehicles and structures*. Beijing: Science Press, (2005).

[18] Y. K. Cheung, F. T. K. Au, D. Y. Zheng and Y. S. Cheng, Vibration of multi-span bridges under moving vehicles and trains by using modified beam vibration functions. *Journal of Sound and Vibration* 228 (1999) 611-628.

[19] A. Matsuura, Study of dynamic behaviors of bridge girders for high-speed railway. *Journal of JSCE* 256 (12) (1976) 35-47.

[20] M. Klasztorny, Vertical vibration of a multi-span bridge under a train moving at high speed. *Proc. EURODYN'99*, Prague, (1999) 651-656.

[21] H. Xia and N. Zhang, Dynamic analysis of railway bridges under high-speed trains. *Computers & Structures*, 83 (2005) 1891-1901.

[22] G. De Roeck, A. Maeck and A. Teughels, Train-bridge interaction validation of numerical models by experiments on high-speed railway bridge in Antoing. *Proc. MCCI'2000*, Beijing, (2000) 61-68.

[23] Japan Subway Association, *Toward the linear metro system age—advantages and issues of linear metro cars: I. Subway*, (1996).

[24] E. L. Wilson, Three-dimensional static and dynamic *analysis of structures*. Berkeley, CA: Computers and Structures Inc., (2002).

[25] W. M. Zhai, *Vehicle-track coupling dynamics*. Beijing: Science Press, (2007).

[26] H. Xia, N. Zhang and W. W. Guo, Analysis of resonance mechanism and conditions of train-bridge system. *Journal of Sound and Vibration*. 297 (2006) 810-822.

He Xia received his MSc degree in Bridge and Tunnel engineering from Northern Jiaotong University in 1984. He then went to the Catholic University of Leuven, Belgium in 1989-1990 as a visiting scholar; the Hong Kong Polytechnic University in 1999-2000 as a research fellow; the Institute of Railway Technology, Japan in 2002 as a visiting scholar, and the University of New South Wales, Australia in 2007 as a visiting Fellow. He is currently a professor at the School of Civil Engineering in Beijing Jiaotong University. Prof. Xia's research interests are in the areas of dynamic interaction analysis of train-bridge system, and railway traffic induced environmental vibrations.